

1 **Realtime measurement of phase partitioning of organic**  
2 **compounds using a Proton-Transfer-Reaction Time-of-Flight**  
3 **Mass Spectrometer coupled to a CHARON inlet**

4 **Yarong Peng<sup>1,2</sup>, Hongli Wang<sup>2,\*</sup>, Yaqin Gao<sup>2</sup>, Shengao Jing<sup>2</sup>, Shuhui Zhu<sup>2</sup>, Dandan**  
5 **Huang<sup>2</sup>, Peizhi Hao<sup>3</sup>, Shengrong Lou<sup>2</sup>, Tiantao Cheng<sup>4,5,\*</sup>, Cheng Huang<sup>2</sup>, Xuan**  
6 **Zhang<sup>3,\*</sup>**

7 <sup>1</sup> Department of Environmental Science and Engineering, Fudan University, Shanghai, 200438, China

8 <sup>2</sup> State Environmental Protection Key Laboratory of Formation and Prevention of Urban Air Pollution  
9 Complex, Shanghai Academy of Environmental Sciences, Shanghai, 200233, China

10 <sup>3</sup> School of Natural Sciences, University of California, Merced, 95343, USA

11 <sup>4</sup> Department of Atmospheric and Oceanic Sciences, Fudan University, Shanghai, 200438, China

12 <sup>5</sup> Big Data Institute for Carbon Emission and Environmental Pollution, Fudan University, Shanghai,  
13 200438, China

14

15 *Correspondence to:* Hongli Wang (wanghl@saes.sh.cn), Tiantao Cheng (ttcheng@fudan.edu.cn), Xuan  
16 Zhang (xzhang87@ucmerced.edu)

17

18 **Abstract.** Understanding the gas-particle partitioning of semivolatile organic compounds  
19 (SVOCs) is of crucial importance in the accurate representation of the global budget of  
20 atmospheric organic aerosols. In this study, we quantified the gas- vs. particle-phase fractions  
21 of a large number of SVOCs in real time in an urban area of East China with the use of a  
22 CChemical Analysis of aeRosols ONline (CHARON) inlet coupled to a high resolution Proton  
23 Transfer Reaction Time-of-Flight Mass Spectrometer (PTR-ToF-MS). We demonstrated the  
24 use of the CHARON inlet for highly efficient collection of particulate SVOCs while  
25 maintaining the intact molecular structures of these compounds. The collected month-long  
26 dataset with hourly resolution allows us to examine the gas-particle partitioning of a variety of  
27 SVOCs under ambient conditions. By comparing the measurements with model predictions  
28 using the instantaneous equilibrium partitioning theory, we found that the dissociation of large  
29 parent molecules during the PTR ionization process likely introduces large uncertainties to the  
30 measured gas- vs. particle-phase fractions of less oxidized SVOCs, and therefore, caution  
31 should be taken when linking the molecular composition to the particle volatility when  
32 interpreting the PTR-ToF-MS data. Our analysis suggests that understanding the fragmentation  
33 mechanism of SVOCs and accounting for the neutral losses of small moieties during the  
34 molecular feature extraction from the raw PTR mass spectra could reduce, to a large extent, the  
35 uncertainties associated with the gas-particle partitioning measurement of SVOCs in the  
36 ambient atmosphere.

37

## 38 **1. Introduction**

39 Gas-particle partitioning of semivolatile organic compounds (SVOCs) is a critical process  
40 involved in the formation and evolution of atmospheric organic aerosols (OA). Traditionally,

41 gas-particle equilibrium partitioning of organic substances is assumed to be established  
42 instantaneously (Zhang and Seinfeld, 2013), this assumption is in question if particles are semi-  
43 solid or glassy (Shiraiwa et al., 2013). Most studies to date addressing the kinetic limitations in  
44 partitioning have used indirect and/or theoretical methods that are lack of chemical and  
45 molecular specificity (Mai et al., 2015; Shiraiwa and Seinfeld, 2012). Direct measurements of  
46 gas-particle partitioning of SVOCs are needed in order to develop accurate parameterizations  
47 for the organic aerosol formation in climate models.

48 The major challenge in the characterization of gas-particle partitioning of SVOCs lies in  
49 the realtime measurement of labile compounds while maintaining their intact molecular  
50 structures with minimal fragmentation (Zhang et al., 2016a; Zhang et al., 2016b; Zhang et al.,  
51 2019). In recent years, soft ionization techniques coupled to mass spectrometry have been  
52 widely used for the measurement of gas-phase SVOCs at the molecular level (Veres et al., 2008;  
53 Crounse et al., 2006; Heald and Kroll, 2020). Combined with thermal desorption methods, these  
54 techniques have also been deployed to measure organic compounds in both gas and particle  
55 phases nearly simultaneously (Krechmer et al., 2016). A notable example would be the use of  
56 the Filter Inlet for Gases and AEROsols coupled with the Chemical Ionization Mass  
57 Spectrometry (FIGAERO-CIMS) to quantify the gas-particle partitioning of a broad range of  
58 organic compounds in real time (Lopez-Hilfiker et al., 2014; Ye et al., 2021; Voliotis et al., 2021;  
59 Wang et al., 2020a; Lutz et al., 2019; Lee et al., 2018; Le Breton et al., 2018; Stark et al., 2017;  
60 Lopez-Hilfiker et al., 2016; Lopez-Hilfiker et al., 2015; Palm et al., 2020). A number of studies  
61 among those have reached a consensus that the thermograms method, i.e., using the calibrated  
62 thermal desorption profiles vs. temperature to derive the volatility, likely provides the best  
63 estimates of the actual phase distribution. In contrast, using the directly measured gas- and

64 particle-phase fractions of a given analyte will most likely introduce a significant positive or  
65 negative bias to the volatility estimation due to the thermal decomposition of labile organic  
66 compounds during the desorption process (Lopez-Hilfiker et al., 2015; Stark et al., 2017). Such  
67 thermal decomposition (or ion fragmentation) artifacts, either positive or negative depending  
68 on the molecular size, have been suggested to constitute the largest uncertainties in the  
69 estimation of phase partitioning behaviors of SVOCs using the thermal desorption method at  
70 ambient pressure (Thompson et al., 2016).

71 Along with the line of thermal desorption method development, an inlet designed for the  
72 CHemical Analysis of aeRosols ONline (CHARON) has been developed and coupled to the  
73 Proton Transfer Reaction Time-of-Flight Mass Spectrometer (PTR-ToF-MS) in recent years.  
74 As CHARON-PTR-ToF-MS does not rely on any form of pre-concentration on surfaces, it  
75 could provide online and direct measurements of organic compounds in both phases, compared  
76 with traditional thermal desorption instruments which still need to address artifacts during the  
77 particle collection and desorption processes. Another potential advantage of CHARON-PTR-  
78 ToF-MS is that the chemical information of the collected particles can be studied qualitatively  
79 and quantitatively over a chemical composition level even at sub-nanogram mass  
80 concentrations per molecule owing to the well studied ion-molecule reaction chemistry in PTR-  
81 ToF-MS (Piel et al., 2019). CHARON has shown promising potential in the realtime analysis  
82 of the chemical composition and spatiotemporal distributions of aerosols with laboratory-,  
83 ground-, and aircraft-based platforms (Piel et al., 2019; Tan et al., 2018; Gkatzelis et al., 2018a;  
84 Gkatzelis et al., 2018b; Muller et al., 2017; Eichler et al., 2017; Eichler et al., 2015; Antonsen  
85 et al., 2017; Leglise et al., 2019; Piel et al., 2021). As a relatively new technique, the use of  
86 CHARON-PTR-ToF-MS to investigate the gas-particle partitioning of organic compounds is

87 still quite limited. Only one study by Gkatzelis et al. (2018b) deployed CHARON, together  
88 with two other aerosol sampling inlets, to measure the OA formation and aging from  
89 monoterpenes and real plant emissions in chamber experiments. Whether the CHARON inlet  
90 can be applied to the study of gas-particle partitioning of organic compounds under the actual  
91 atmospheric conditions remains to be validated.

92 In this study, we assess the applicability of the CHARON inlet to the time-resolved  
93 collection of organic compounds in their native molecular state using laboratory tests with a  
94 series of authentic standards. We further employ the CHARON inlet coupled to a high  
95 resolution PTR-ToF-MS instrument to measure an array of gaseous and particulate SVOCs in  
96 an urban area of East China. The obtained month-long hourly dataset allows us to examine the  
97 gas-particle partitioning of SVOCs spanning a range of volatilities. By comparing the  
98 measurements with model predictions using the instantaneous equilibrium partitioning theory,  
99 we found that fragmentation during the PTR ionization process may introduce large  
100 uncertainties to the measured gas- vs. particle-phase fractions of less oxidized SVOCs.  
101 Understanding the dissociation patterns of parent molecules and accounting for the  
102 fragmentation losses when extracting the molecular features from the raw PTR mass spectra  
103 are needed to improve the measured accuracy of SVOCs partitioning between the gas and  
104 particle phase.

105

## 106 **2. Material and Methods**

### 107 **2.1. Sampling site**

108 The sampling site located in the campus of the Shanghai Academy of Environmental  
109 Science (SAES) is representative of a typical urban setting surrounded by restaurants, shopping

110 malls, and residential and commercial buildings (Fig. S1). Two traffic-heavy streets in the area  
111 (Caobao Road and Humin Highway) are located  $\sim$  150 m and 450 m lateral distances to the east  
112 of the sampling site. A few number of petrochemical and chemical industrial facilities are  
113 located  $\sim$  50 km to the south and southwest of the observation site, which likely bring certain  
114 long-lived pollutants to the site at a typical wind speed of  $\sim$  1 – 3 m/s. Major pollution sources  
115 in the area include traffic, commercial and residential activities, and regional transport (Huang  
116 et al., 2021; Peng et al., 2023). The sampling inlet of the PTR-ToF-MS instrument was installed  
117 on the roof of an eight-story building  $\sim$  24 m above the ground. A comprehensive measurement  
118 of gas- and particle-phase compounds in the ambient air was performed from Oct 24 to Nov 22.  
119 During the sampling period, the average temperature, relative humidity, and wind speed were  
120  $18.0 \pm 3.0$  °C,  $61.0 \pm 15.0\%$ , and  $1.8 \pm 0.7$  m/s, respectively. The prevailing wind direction in  
121 this region was from the northwest and north during the polluted period (Fig. S2).

## 122 **2.2. CHARON-PTR-ToF-MS**

### 123 **2.2.1. Operation protocols**

124 A Proton Transfer Reaction Time-of-Flight Mass Spectrometer (PTR-ToF-MS) coupled to  
125 a CChemical Analysis of aeRosols ONline (CHARON, Ionicon Analytik Inc, Innsbrunck,  
126 Austria) inlet was employed to measure the gas- and particle-phase concentrations of a series  
127 of SVOCs. The PTR-ToF-MS instrument used here is equipped with a radio frequency (RF)-  
128 only quadrupole ion guide that transmits ions more efficiently (PTR-QiTof, Ionicon Analytik  
129 Inc). The operating parameters of the PTR-ToF-MS were held constant during the entire  
130 measurement period. The drift tube pressure, temperature, and voltage were 2.9 mbar, 120 °C,  
131 and 500 V, respectively. These conditions correspond to an  $E/N$  ( $E$  is the electric field, and  $N$  is  
132 the number density of the gas molecules in the drift tube) value of  $\sim$  100 Td (1 Td =  $10^{-17}$  V

133  $\text{cm}^2$ ) and a reaction time of 120  $\mu\text{s}$ . Note that the  $E/N$  value determines the collision energy of  
134 ions in the reactor and therefore the degree of fragmentation and cluster formation. The  
135 operating conditions were selected for the purpose of relatively low fragmentation intensities  
136 (compared to 120 – 140 Td) and limited production of water clusters (compared to 60 – 80 Td).  
137 Low  $E/N$  enhances the degree of water clustering, which complicates the analysis of analyte  
138 ions due to a complex interplay between cluster formation ( $\text{RH}^+(\text{H}_2\text{O})_n$ ) and proton transfer  
139 reactions (Holzinger et al., 2019). During the campaign, the sensitivity of the PTR-ToF-MS  
140 was in the range of 300 – 1000 ncps  $\text{ppb}^{-1}$  and the mass resolution was maintained at  $\sim 5000$   
141  $\text{m}/\Delta\text{m}$ . Mass spectra were collected at a time resolution of 10 s.

142 The CHARON inlet consists of 1) a gas-phase denuder (GPD) for stripping off gas-phase  
143 analytes, 2) an aerodynamic lens (ADL) for particle collimation which is combined with an  
144 inertial sampler for emanating the particle-enriched flow, and 3) a thermo-desorption unit (TDU)  
145 for particle volatilization. The CHARON inlet functionality has been described in great detail  
146 by Eichler et al. (2015). The inlet we used here had a particle enrichment factor of  $\sim 15$ , as  
147 discussed shortly. The vaporizer (TDU) was operated at 140  $^{\circ}\text{C}$  and  $\sim 8$  mbar absolute pressure.  
148 Measurements of organic compounds in the gas and particle phase were conducted using a  
149 parallel sampling system with two independent pumps, allowing for the selection of flow rates  
150 specifically adjusted for each phase, resulting in the overall residence time of less than 2 s (Fig.  
151 S3).

152 **2.2.2. Sampling alternation between gas and particle phase**

153 Gas-phase compounds were measured by directly sampling the ambient air via a 2 m long  
154 perfluoro-alkoxy (PFA) tube (1/4" OD) capped with a polytetrafluoroethylene (PTFE) filter  
155 (Mitex<sup>TM</sup> PTFE membrane, 5  $\mu\text{m}$  pore size, 47 mm diameter) to prevent the clogging of

156 particles in the PTR capillaries. The gas-phase inlet was independently connected to the PTR-  
157 ToF-MS instrument upstream of the drift tube via a pressure-controlled subsampling PEEK  
158 capillary (1/16" OD). Zero measurements were performed by overflowing catalytically  
159 (platinum at 370°C) purified air through the inlet. Ambient particles were sampled through a  
160 stainless steel tube (3/8" OD) with a flow rate of  $\sim 3 \text{ L min}^{-1}$ , out of which a flow of  $\sim 500 \text{ ml}$   
161  $\text{min}^{-1}$  was directed to the CHARON inlet. A PM<sub>2.5</sub> cyclone was installed in front of the sampling  
162 line to remove coarse particles ( $> 2.5 \mu\text{m}$ ). The particle-phase background was measured by  
163 placing a High-Efficiency Particulate Air filter (HEPA, HEPA-CAP 7, GE Healthcare UK  
164 Limited, Buckinghamshire, UK) upstream of the CHARON inlet. Servo motor activated valves  
165 made of passivated stainless steel were used for switching between the two inlet configurations.  
166 During the campaign, CHARON-PTR-ToF-MS automatically switched between gas and  
167 particle phase every 15 min. Detailed setup is given in Fig. S3 in the Supporting Information.

168 The built-in PTR-manager software (Ionicon Analytik GmbH, Innsbruck, Austria) offers  
169 the possibility to program sequences by which the instrument switches between different  
170 settings. It takes  $\sim 1 \text{ min}$  for gases and particles to re-equilibrate when switching between these  
171 two modes. Data generated during this transition period ( $\sim 2 \text{ min}$ ) were not considered.  
172 Instrument background was measured for 15 min every 5h. The limits of detection (LoD) at 1  
173 min resolution were in the range of  $5.6 \pm 2.9 \text{ ng m}^{-3}$  for gases and  $0.7 \pm 0.5 \text{ ng m}^{-3}$  for particles,  
174 respectively (Fig. S5). Concentrations of gaseous and particulate compounds shown here  
175 included the last 5 min of every gas/particle-phase working mode, in order to minimize the  
176 interferences carried over from the previous working mode by allowing for a sufficient amount  
177 of equilibration time in the inlet (Piel et al., 2021). In order to synchronize the gas- and particle-  
178 phase data to calculate gas-particle partitioning, the average hourly data were then used for

179 further analysis.

180 **2.2.3. Sensitivity and calibration**

181 Weekly calibrations were performed using a multicomponent calibration gas standard  
182 (Linde, USA) at five concentration levels from 0.5 to 10 ppb (Fig. S4a). The calibration mixture  
183 includes methanol, acetonitrile, acetaldehyde, acrolein, acetone, isoprene, methyl vinyl ketone,  
184 methyl ethyl ketone, 2-pentanone, toluene, styrene, p-xylene, 1,3,5-trimethylbenzene,  
185 naphthalene and  $\alpha$ -pinene. Here the sensitivity of PTR-ToF-MS is defined as the normalized  
186 ion intensity of  $\text{RH}^+$  (ncps) obtained at a mixing ratio of 1 ppb. For a given species ( $R$ ), its  
187 sensitivity ( $S$ , ncps ppb $^{-1}$ ) is a linear function of the rate constant of its reaction with  $\text{H}_3\text{O}^+$  ( $k$ ) :

$$188 S = \frac{\frac{I_{\text{RH}^+}}{I_{\text{H}_3\text{O}^+}} \times 10^6}{\frac{[R]}{N} \times 10^9} = k \times N \times 10^{-3} \times t \times \frac{T_{\text{RH}^+}}{T_{\text{H}_3\text{O}^+}} \times F_{\text{RH}^+} \quad (1)$$

$$189 \text{corrected } S = \frac{S}{\frac{T_{\text{RH}^+}}{T_{\text{H}_3\text{O}^+}} \times F_{\text{RH}^+}} = a \times k \quad (2)$$

190 where the signals of  $\text{H}_3\text{O}^+$  ( $I_{\text{H}_3\text{O}^+}$ ) and  $\text{RH}^+$  ions ( $I_{\text{RH}^+}$ ) measured by the mass analyzer (in cps)  
191 can be related to the signals of  $\text{H}_3\text{O}^+$  ( $[\text{H}_3\text{O}^+]$ ) and  $\text{RH}^+$  ( $[\text{RH}^+]$ ) ions at the end of the drift tube,  
192 using their respective transmission efficiencies ( $T_{\text{H}_3\text{O}^+}$  and  $T_{\text{RH}^+}$ ) from the drift tube to the  
193 detector (De Gouw and Warneke, 2007).  $[R]$  is the concentration of species  $R$  and  $N$  is the  
194 number density of gas in the drift tube. The reaction time ( $t$ ) is determined by the ion drift  
195 velocity.  $F_{\text{RH}^+}$  represents the fraction of product ions detected as  $\text{RH}^+$  ions ( $0 \leq F_{\text{RH}^+} \leq 1$ ). For  
196 non-fragmenting compounds,  $F_{\text{RH}^+} = 1$ . The measured sensitivity is further corrected by  
197 accounting for fragmentation and transmission efficiency. The relative transmission efficiency  
198 of ions was derived from laboratory experiments (Fig. S4a).  $a$  is the slope of the linear  
199 regression of the corrected sensitivities on the proton-transfer-reaction rate coefficients ( $k$ ), as

200 shown in Fig. S4b. Following the method by Sekimoto et al. (2017), the linear regression result  
201 was used to determine the sensitivities of all uncalibrated species. The overall uncertainty was  
202 less than 15% for compounds with standards and around 50% for those without standards.  
203 Calculated sensitivity based on this method agrees well with measurements of authentic  
204 standards (Fig. S4c).

205 **2.2.4. Enrichment factor**

206 The CHARON inlet was calibrated routinely with pure ammonium nitrate particles to  
207 derive the enrichment factor as a function of the particle size following the procedures described  
208 in Eichler et al. (2015). In addition, we used a selection of authentic standards (Table S1) to test  
209 the effect of desorption temperature on the enrichment factor of labile compounds. Previous  
210 studies with CHARON generally used a temperature of 140 °C to vaporize particles (Leglise et  
211 al., 2019; Gkatzelis et al., 2018b; Tan et al., 2018). Herein, we tested the TDU temperature  
212 ranging from 70 to 140°C. The selected chemical standards were individually dissolved in  
213 distilled water (ethanol in the case of 2-Pentadecanone and 1-Pentadecanol) and nebulized by  
214 an atomizer (TSI 3076, Shore-view, MN, USA) that was pressurized with ultrapure zero air.  
215 The nebulizer outflow was diverted through two diffusion dryers to remove water vapor and an  
216 activated charcoal denuder (NovaCarb F, Mast Carbon International Ltd., Guilford, UK) to  
217 remove organic vapors. The resulting flow of polydisperse particles was then delivered into a  
218 differential mobility analyzer (DMA, TSI 3080) for particle size selection. The transmitted  
219 particles at a given size bin (300 nm for organics and 100 – 450 nm range for ammonium nitrate)  
220 were introduced into the CHARON-PTR-ToF-MS analyzer and a condensation particle counter  
221 (CPC, TSI 3775), respectively. Particle mass concentrations were calculated based on the CPC  
222 number distribution measurements by assuming a shape factor of 0.8 for ammonium nitrate

223 particles and 1 for organic particles, respectively.

224 The particle enrichment factor ( $EF$ ) of a given analyte  $i$  was calculated as the ratio of the  
225 PTR-ToF-MS derived vs. CPC derived mass concentrations of analyte  $i$  at a given particle size  
226 bin:

$$227 \quad VMR_{(PTR)i} = \frac{I_i}{S_i} \quad (3)$$

$$228 \quad VMR_{(CPC)i} = \rho_i \times V \times N_i \times V_m / Mw_i \quad (4)$$

$$229 \quad EF = \frac{VMR_{(PTR)i}}{VMR_{(CPC)i}} \quad (5)$$

230 where  $I_i$  is the normalized signal of species  $i$  (ncps) by PTR-ToF-MS,  $S_i$  is the sensitivity  
231 (ncps ppb $^{-1}$ ),  $VMR$  is the volume mixing ratio (ppb),  $\rho$  is the density of species  $i$  (g cm $^{-3}$ ),  
232  $V$  is the volume of a particle sphere (m $^3$ ),  $N_i$  is the number concentration of particles measured  
233 by CPC (cm $^{-3}$ ),  $V_m$  is the molar volume of an ideal gas at 1 atm (22.4 L mol $^{-1}$ ),  $Mw_i$  is the  
234 molecular weight (g mol $^{-1}$ ). As the calculated sensitivities of most organics in the absence of  
235 authentic standards are subject to uncertainties (15% – 50%), we will herein use the  
236 multiplication of  $EF$  and  $S_i$  to evaluate the combined effect of CHARON enrichment and  
237 sensitivity on the measured concentrations of a given analyte  $i$  in the particle phase.

### 238 2.2.5. Data processing

239 Data were analyzed using the Tofware package (v3.2.0, Tofwerk Inc), within the Igor Pro  
240 software (v7.0, Wavemetrics). Using this package, time-dependent mass calibrations were  
241 performed using four ions ( $H_3^{18}O^+$ ,  $NO^+$ ,  $C_6H_5I^+$  and  $C_6H_5I_2^+$ ), where  $C_6H_5I^+$  and  $C_6H_5I_2^+$  were  
242 produced from the internal standard di-iodobenzene. The relative mass deviation was within 6  
243 – 8 ppm across the mass spectra. Considering the humidity dependence of reagent ions ( $H_3O^+$   
244 and  $H_3O^+(H_2O)$ ), the fitted product ion signals ( $RH^+$ ) were normalized to a standard reagent ion

245 of  $10^6$  cps (counts per second). Elemental composition was determined based on the accurate  
246 *m/z* (mass to charge ratio) and isotopic pattern analysis. A list of  $\sim 1600$  ions was extracted,  
247 including both gas- and particle-phase ions. Molecular formulas including only C, H, and O  
248 atoms were assigned to the detected ions by the addition of one proton in cases where the  
249 elemental composition analysis returned multiple options. About 85% of the signals were  
250 elementally resolved by the  $C_xH_yO_z$  formula in ambient air mass spectra. A small number of  
251 nitrogen containing compounds, such as nitroaromatics, were also identified but not included  
252 in the following analysis. Throughout of the context, we use the word “species” to refer to all  
253 compounds with assigned molecular formula, which may include multiple isomers.

254 **2.3. Complementary measurements**

255 In addition to CHARON-PTR-ToF-MS, a Thermal desorption Aerosol Gas chromatograph  
256 (TAG) was also employed to measure a series of particle-phase organic species. Details of the  
257 TAG operation and data analysis protocols can be found in previous studies (He et al., 2020;  
258 Wang et al., 2020b; Zhu et al., 2021). The elemental composition and mass concentration of  
259 particles were measured by an Aerodyne high-resolution time-of-flight Aerosol Mass  
260 Spectrometer (AMS), with details of operation and quality control protocols given by our recent  
261 study (Huang et al., 2021). Volatile organic compounds (VOCs,  $C_2 - C_{12}$ ) were analyzed by a  
262 custom-built online gas chromatography system equipped with a mass spectrometer and a flame  
263 ionization detector (GC-MS/FID). The performance of this system can be found in our previous  
264 publications (Zhu et al., 2018; Wang et al., 2014). Meteorological parameters (ambient  
265 temperature, wind speed, wind direction, and relative humidity) were collected by an automatic  
266 weather station (Metone 590 series) mounted on the roof top of the campaign site.

267 **2.4. Gas-particle partitioning measurements vs. modeling**

268 The CHARON-PTR-ToF-MS measured gas- and particle-phase concentrations of a given  
 269 species  $i$  can be used to calculate its particle-phase fraction ( $F_{p,i}$ ).

270 
$$P_i = \frac{\frac{I_{p,i} \times \left(\frac{m}{z_i} - 1\right)}{V_m \times S_i}}{EF} \quad (6)$$

271 
$$G_i = \frac{I_{g,i} \times \left(\frac{m}{z_i} - 1\right)}{V_m \times S_i} \quad (7)$$

272 
$$F_{p,i} = \frac{P_i}{P_i + G_i} \quad (8)$$

273 where  $P_i$  and  $G_i$  are the mass concentrations ( $\text{ng m}^{-3}$ ) of species  $i$  in the particle and gas  
 274 phase, respectively.  $I_{p,i}$  and  $I_{g,i}$  are the normalized signal (ncps) of the PTR-ToF-MS detected  
 275 ion  $i$  in the particle and gas phase, respectively.  $V_m$  is taken as  $22.4 \text{ L/mol}$ .  $S_i$  is calculated  
 276 or measured sensitivity (ncps  $\text{ppb}^{-1}$ ), see details in Section 2.2.3. As structural isomers cannot  
 277 be resolved in the mass spectra, the calculation here assumes that all isomers with the same  
 278 molecular formula have the same chemical properties, i.e., saturation vapor pressures.  
 279 Substitution of Equations (6) and (7) to Equation (8) yields the final expression of the particle-  
 280 phase fraction of species  $i$  ( $F_{p,i}$ ), which is a function of the observed PTR-MS raw signals of  
 281 species  $i$  in the gas and particle phase (in total ion counts), as well as the particle enrichment  
 282 factor ( $EF$ ) of species  $i$ .

283 
$$F_{p,i} = \frac{I_{p,i}/EF}{I_{p,i}/EF + I_{g,i}} \quad (9)$$

284 Gas-particle partitioning of a given analyte  $i$  was also modeled using the equilibrium  
 285 partitioning theory (Pankow, 1994):

286 
$$F_{p,i} = \frac{1}{1 + C_i^* / C_{OA}} \quad (10)$$

287 
$$C_i^* = \frac{10^6 Mw_i \zeta p_i}{RT} \quad (11)$$

288 where  $C_{OA}$  is the organic aerosol concentration measured by AMS ( $\mu\text{g m}^{-3}$ ),  $C_i^*$  is the  
 289 saturation mass concentration ( $\mu\text{g m}^{-3}$ ),  $Mw_i$  is the molecular weight ( $\text{g mol}^{-1}$ ),  $\zeta$  is the  
 290 activity coefficient (assumed as unity),  $p_i$  is the pure component liquid vapor pressure (Pa),  $R$   
 291 is the universal gas constant ( $8.2 \times 10^{-5} \text{ m}^3 \text{ atm K}^{-1} \text{ mol}^{-1}$ ), and  $T$  is the ambient temperature  
 292 (K). As detailed chemical information is lacking for all species detected by PTR-ToF-MS, here  
 293 we use the expression given by Donahue et al. (2011) to approximate the value of  $C_i^*$ :

294 
$$\log_{10} C_i^* = (n_C^0 - n_C^i) b_C - n_O^i b_O - 2 \frac{n_C^i n_O^i}{n_C^i + n_O^i} b_{CO} \quad (12)$$

295 where  $n_C^0 = 25$ ,  $b_C = 0.475$ ,  $b_O = 2.3$ , and  $b_{CO} = -0.3$ .

296

297 **2.5. Uncertainties in the measured and modeled gas-particle partitioning**

298 The uncertainty associated with the PTR-MS measured concentrations in both gas and  
 299 particle phases is less than 15% for compounds with chemical standards based on the optimally  
 300 fitted transmission efficiency curve. For those in the absence of standards, their PTR  
 301 sensitivities were calculated theoretically using Equations (1-2), and the uncertainty in the  
 302 calculation mainly arises from the estimation of polarizability and dipole moment of the target  
 303 molecule, which has been estimated to be within  $\sim 50\%$  when only the elemental composition  
 304 of that molecule is given (Sekimoto et al., 2017). It is important to note, however, that the  
 305 uncertainty associated with the estimated PTR sensitivity has zero influence on the measured  
 306 particle-phase fraction of any given compound because the sensitivity term is essentially  
 307 canceled in the divisor function in Equation (9). The uncertainty associated with the particle  
 308 fraction of a given species  $i$  derived from the PTR-MS measurements arises predominantly

309 from the “*EF*” term. Since the uncertainty of the measured *EF* depends on the uncertainty of  
310  $I_{p,i}$ , we thus express the overall uncertainties of the measured gas-particle partitioning as:

311 
$$Unc(F_{p,i}) = \sqrt{Unc(EF)^2 + Unc(I_{g,i})^2} \quad (13)$$

312 with the calibration standards used in this study, the enrichment factor is calculated to be within  
313 25% error (*Unc(EF)*) (see detailed calculations listed in Table S2 and S3), including the effect  
314 of wall loss inside the inlet tubing and the precision of the measurement. Huang et al. (2019)  
315 has tested the uncertainty of wall loss (*Unc(I<sub>g,i</sub>)*) in this PTR-MS instrument as 28%. Therefore,  
316 the overall uncertainty in the measured particle-phase fraction (*Unc(F<sub>p,i</sub>)*) was estimated as  
317 38%.

318 The uncertainty associated with the modeled gas-particle partitioning arises primarily from  
319 the uncertainty in the estimation of the saturation mass concentration ( $C_i^*$ ) based on the method  
320 developed by Donahue et al. (2011). In this method, the saturation mass concentration of  
321 species *i* is a non-linear function of the numbers of carbon and oxygen atoms in that particular  
322 species, see Equation (12). For each generic molecular formula, i.e.,  $C_xH_y$ ,  $C_xH_yO$ ,  $C_xH_yO_2$ , and  
323  $C_xH_yO_4$ , Donahue et al. (2011) have used a total of 25, 48, 18, and 10 chemical standards with  
324 known volatilities to validate the estimated saturation concentrations, and the estimated errors  
325 were taken as 34%, 16%, 25%, and 54%, respectively (see Table S6). As the  $C_xH_yO_3$  group was  
326 not tested, we tentatively assumed the associated errors as the same as the  $C_xH_yO_4$  group. The  
327 extent to which these uncertainties may affect the difference between measurements and model  
328 results was discussed in detail in the Supporting Information (Fig. S10).

329

330 **3. Results and Discussion**

331 **3.1. Particle enrichment: effect of desorption temperature**

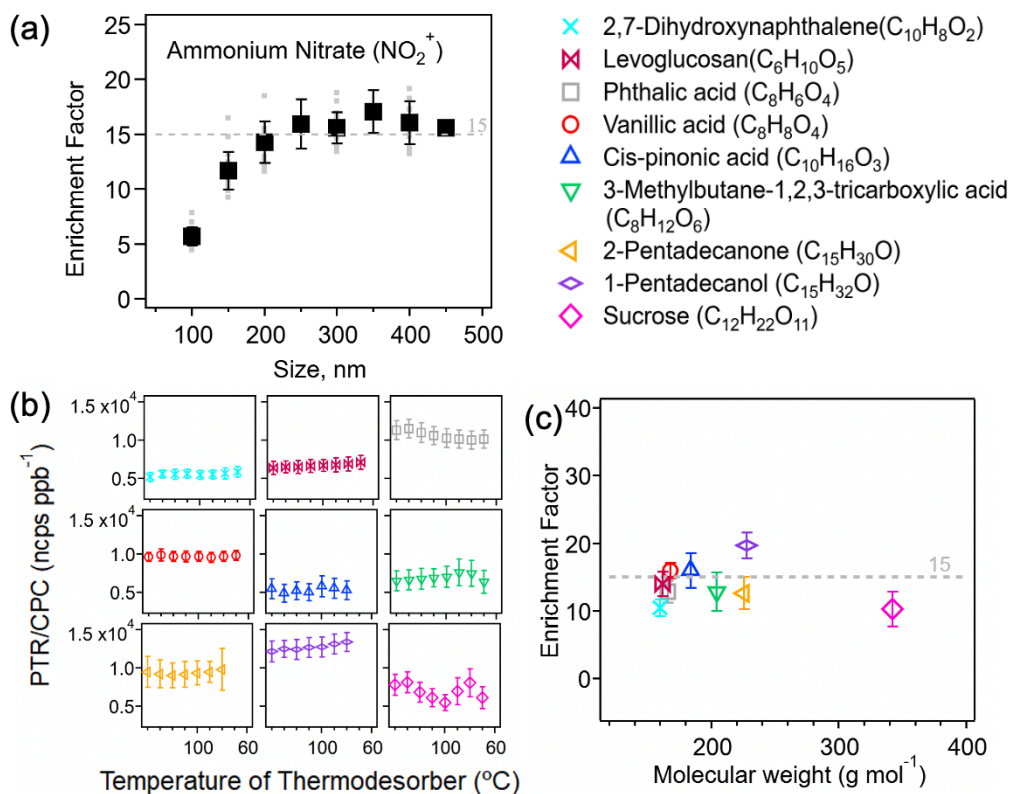
332 Thermal desorption as a common procedure used in the chemical characterization of  
333 organic aerosols is often susceptible to fragmentation of non-refractory compounds. Due to the  
334 high temperature used to evaporate particles collected, labile and large molecules are inevitably  
335 subject to fragmentation, thereby introducing large uncertainties to the measured mass and  
336 composition of the particulate organic compounds (Lopez-Hilfiker et al., 2015; Yatavelli et al.,  
337 2012; Zhao et al., 2013). Thermal decomposition of oxidized organic compounds has been  
338 observed at vaporizer temperature as low as 200 °C, the lowest temperature required to vaporize  
339 OA as reported (Stark et al., 2017). While decreasing the vaporizer temperature is necessary to  
340 maintain the intact structure of labile molecules, low temperature (e.g., 85 °C), however, might  
341 fail to completely evaporate the collected particles into vapors, resulting in an underestimation  
342 of the collected OA mass (Inomata et al., 2014). Here we performed a series of sensitivity tests  
343 to identify the optimal vaporizer temperature in the CHARON inlet for the measurements of  
344 organic compounds in the particle phase.

345 Prior to the temperature sensitivity test, we have validated that the particle enrichment  
346 factor, also known as collection efficiency and defined as the ratio of the particle mass  
347 concentration upstream to downstream of the aerodynamic lens, does not depend on the particle  
348 size. As shown in Fig. 1a, the measured *EF* value for ammonium nitrate particles, detected as  
349  $\text{NO}_2^+$  produced from the nitric acid vapor, remains constant as ~ 15 in the 150 – 450 nm particle  
350 size range. The lower values in the 100 – 150 nm size range can be explained by the lower  
351 particle transmission efficiency in the gas phase denuder, e.g., 75% – 80% for 100 nm particles  
352 (Eichler et al., 2015). Also, particles below 150 nm are less efficiently concentrated in the

353 subsampling flow after the aerodynamic lens. Therefore, we used the monodisperse particles  
354 generated from selected organic standards at 300 nm for the temperature sensitivity test.

355 A number of chemical standards that are representative of alcohols, carbonyls, and  
356 carboxylic acids and with the vapor pressure ranging from  $10^{-14}$  to  $10^{-1}$  Pa at 25 °C (taken from  
357 EPA EPI Suite (2012), see values given in Table S1) were used to generate organic aerosols,  
358 which, upon size selection at 300 nm, were directed to the CHARON inlet. Particle evaporation  
359 occurs downstream of the aerodynamic lens in the gas phase and on the tube and orifice surface  
360 to which submicron particles rapidly diffuse at  $\sim 8$  mbar operating pressure. The thermal  
361 desorption unit was designed to ensure that ammonium sulfate particles ( $10^{-20}$  Pa) can be  
362 completely evaporated (Piel et al., 2019; Eichler et al., 2015). As the desorption temperature  
363 was varied from 70 °C to 140 °C, the intensities of all detected ions (including both parent and  
364 fragment ions) for each organic standard analyzed were stable within 15%, as shown in Fig. 1b.  
365 Also note that we did not observe any ions produced from decarboxylation and/or dehydration  
366 during the particle evaporation process. This is because the relative low operation temperature  
367 and the short heat exposure time could effectively limit any thermal dissociation of organic  
368 molecules. This demonstrates that the parent molecule fragmentation, if any, does not occur  
369 under the range of desorption temperature used in the CHARON inlet, but rather results from  
370 the ionic dissociation process in the PTR ionization chamber, see more discussions in Section  
371 3.3. We therefore used the sum total of intensities of all major ions detected as the PTR-ToF-  
372 MS response to a given organic standard analyzed. Fig. 1c shows that the derived enrichment  
373 factors stay constant for all compounds investigated ( $Mw \sim 160 - 230$  g/mol). The relative  
374 signals of all fragment ions were stable over the range of the desorption temperature as shown  
375 in Fig. 2. This suggests that the desorption temperature used here, even as low as 70 °C, is

376 sufficient to evaporate SVOCs (volatility  $> 10^{-14}$  Pa at 25 °C), due to the low operating pressure  
 377 (~ 8 mbar) that significantly enhances the partitioning shift to the gas phase. One low volatility  
 378 compound, sucrose ( $M_w$  is 342 g/mol and vapor pressure is  $4.69 \times 10^{-14}$  Pa), has a slightly lower  
 379 enhancement factor compared with all the other organic standards tested. This is mainly due to  
 380 the intensive dehydration of the parent compound in the ionization chamber, and as a result,  
 381 only a few fragment ions were captured, resulting in a lower PTR response and thereby lower  
 382  $EF$  value calculated from Equations (3-5). The  $EF$  values of sucrose also have much higher  
 383 standard deviations at all temperatures due to fragmentation (Table S3).

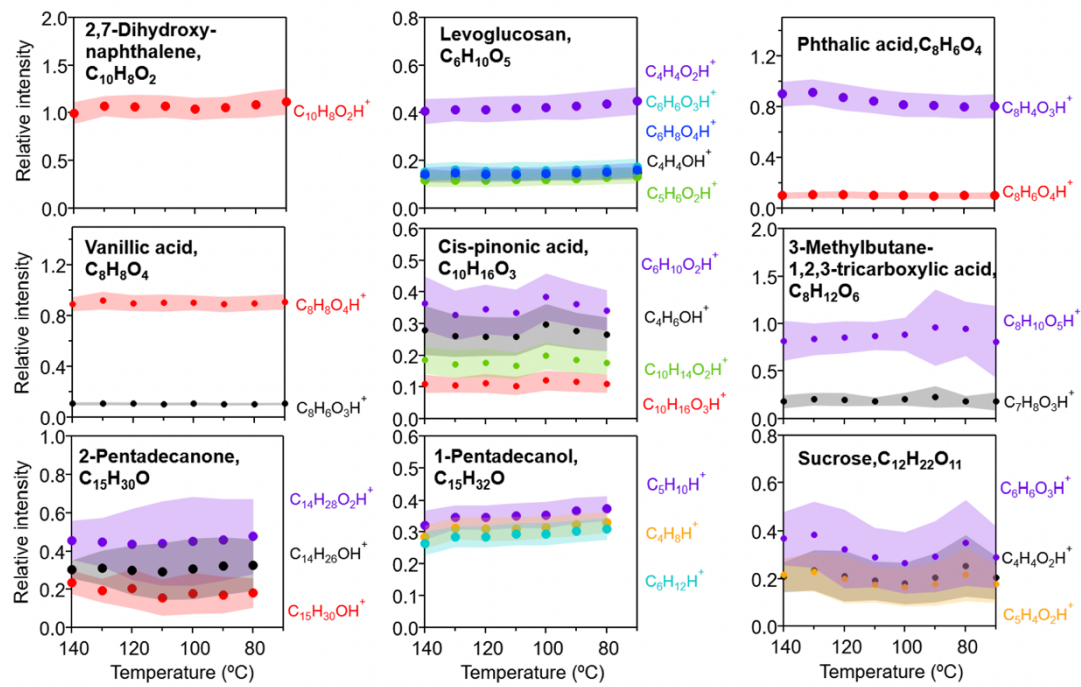


384

385 Figure 1. (a) Measured unitless enrichment factor ( $EF$ ) of ammonium nitrate particles as a

386 function of particle size in the 100 – 450 nm range. Grey markers represent all replicating  
 387 measurements. The error bar denotes one standard deviation ( $1\sigma$ ) of the average. (b) Ratios of  
 388 PTR-ToF-MS signals (including both parent and fragment ions) to CPC counts ( $\pm 1\sigma$ ) at 300  
 389 nm for all organic standards studied. (c)  $EF$  ( $\pm 1\sigma$ ) of selected organic standards based on the  
 390 calculated sensitivity.

391



392

393 Figure 2. Ratios of CHARON-PTR-ToF-MS signals (ncps) to CPC measurements (ppb) of all  
 394 detected ions (including both parents and fragments) for a given pure organic standard tested  
 395 under different desorption temperatures (70 – 140 °C), normalized to the corresponding ratios  
 396 obtained at 140 °C. Ions with relative intensities less than 10% are excluded. Red markers  
 397 represent the parent peaks. Colored shades represent the relative standard deviations at different

398 temperatures (exact values are given in Table S4).

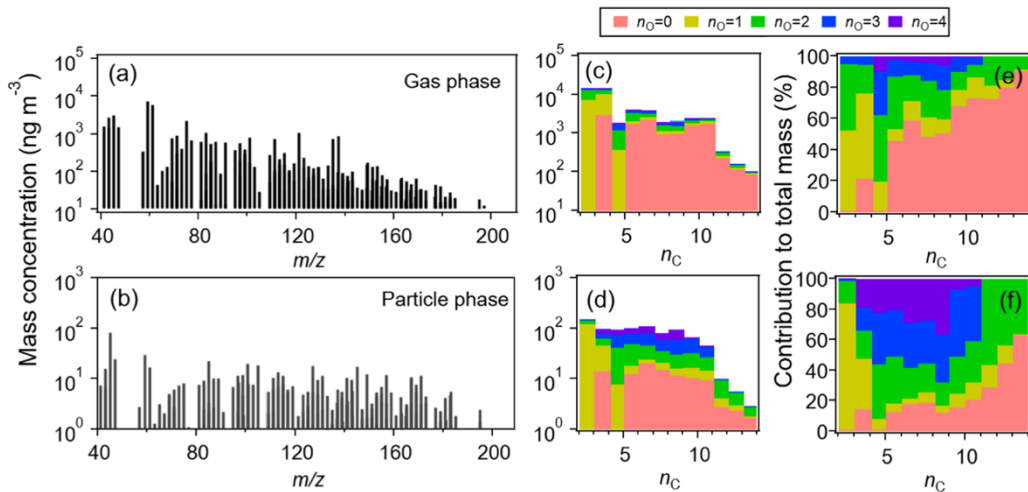
399 It has been recognized that species with one functional group follow certain fragmentation  
400 patterns during the PTR ionization process (Pagonis et al., 2019; Francis et al., 2007; Spanel et  
401 al., 1997; Tani et al., 2003; Spanel and Smith, 1997), such as dehydration of acids and alcohols.  
402 The observed dissociation of carboxylic acid standards used in this study, e.g., phthalic acid  
403 and 3-methylbutane-1,2,3-tricarboxylic acid, can be explained by this common fragmentation  
404 pattern. The fragmentation mechanism of muti-functionalized species is rather complicated and  
405 a number of fragments can be produced upon PTR ionization. Nevertheless, the identity and  
406 abundance of fragments from a given muti-functionalized species have been found comparable  
407 under the same PTR operation protocols (Leglise et al., 2019; Gkatzelis et al., 2018a). For  
408 example, *cis*-pinonic acid yields the following fragments (main ions only and relative  
409 abundance in parentheses):  $m/z$  71.049 (~28%), 115.075 (~36%), 167.108 (~19%), and 185.117  
410 (~11%), which is comparable with an earlier study (Leglise et al., 2019):  $m/z$  71.049 (~27%),  
411 115.075 (~33%), 167.108 (~26%), and 185.117 (~14%) at 100 Td settings.

412

### 413 **3.2. Molecular features of detected organic species**

414 A month-long field dataset of particle- and gas-phase organic species was collected at  
415 hourly resolution using the CHARON-PTR-ToF-MS instrument. A comparison of PTR-ToF-  
416 MS measurements with other techniques available on site was performed for both gas and  
417 particle phases. For the gas phase, quantitative measurements of a suite of VOCs by GC-  
418 MS/FID, including benzene, toluene, styrene, C<sub>8</sub> and C<sub>9</sub> aromatics, acrolein, and C<sub>4</sub>, C<sub>5</sub>, and C<sub>6</sub>  
419 ketones, agree well with corresponding PTR-ToF-MS measurements, as shown in Fig. S6. For  
420 the particle phase, the time series of a group of C<sub>x</sub>H<sub>y</sub>O<sub>4</sub> species (including C<sub>4</sub>H<sub>6</sub>O<sub>4</sub>, C<sub>5</sub>H<sub>8</sub>O<sub>4</sub>,

421  $C_6H_{10}O_4$ , and  $C_8H_6O_4$ ) are in reasonable agreement with corresponding measurements taken by  
 422 TAG ( $r \sim 0.60 - 0.80$ ), although the CHARON-PTR-ToF-MS measured total molecular mass  
 423 is generally lower than the TAG measurements by a factor of 2 to 6 (Fig. S7). This is likely  
 424 caused by the fragmentation (e.g., loss of  $H_2O$ , see Fig. S8) of the parent compounds during the  
 425 ionization process, as discussed in detail in Section 3.3. The time series of total OA mass  
 426 characterized by CHARON-PTR-ToF-MS also agree with the AMS measurements ( $r \sim 0.91$ ,  
 427 Fig. S9). Previous studies have reported the particulate organics measured by PTR-MS with a  
 428 thermal desorption inlect account for 25% – 60% mass of the total organic aerosols measured  
 429 by AMS (Holzinger et al., 2013). Direct comparison of the total OA mass loading is not  
 430 applicable here since the CHARON-PTR-ToF-MS measurement only focused on compounds  
 431 with the mass to charge ratio below 300 Th. That the majority of ions detected by PTR are  
 432 present in the lower mass range is primarily due to the fragmentation of larger masses during  
 433 the ionization process, as discussed extensively in Section 3.3.



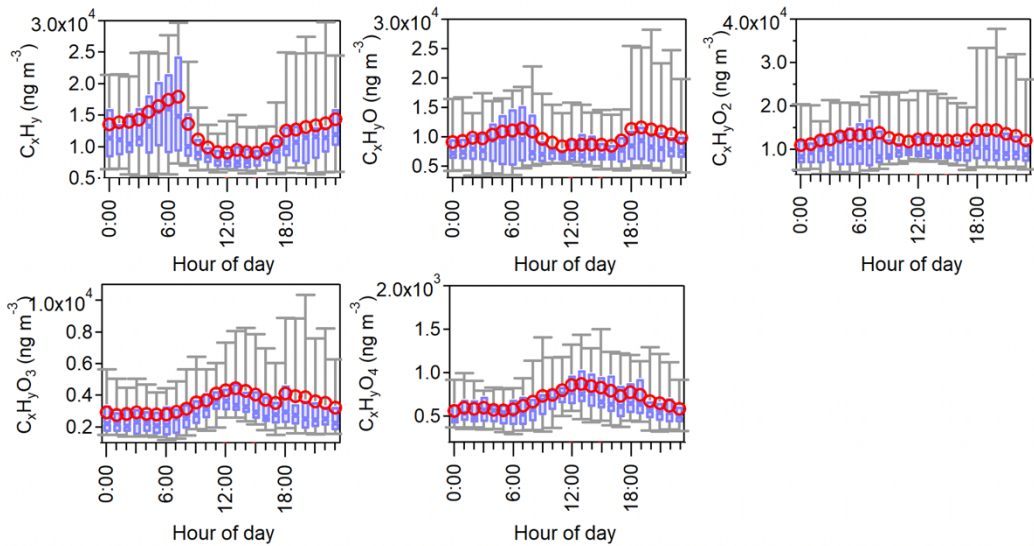
434  
 435 Figure 3. Background subtracted monthly-average PTR-ToF-MS mass spectra in the (a) gas  
 436 phase and (b) particle phase. Mass distributions of all identified species resolved by the carbon

437 and oxygen numbers ( $n_C$  and  $n_O$ ) in the (c) gas phase and (d) particle phase, as well as their  
438 relative contribution to the total organic mass in the (e) gas phase and (f) particle phase.

439

440 Fig. 3 (a-b) shows the PTR-ToF-MS spectra of dominant ions averaged over the entire  
441 campaign in both gas and particle phases. The mass concentrations of individual ions are in the  
442 range of  $7.9 - 7179.3 \text{ ng m}^{-3}$  in the gas phase and  $0.6 - 82.7 \text{ ng m}^{-3}$  in the particle phase. A total  
443 of 152 species (with  $> 60\%$  data points above the PTR-ToF-MS detection limits) are identified,  
444 contributing to  $\sim 69\%$  and  $\sim 44\%$ , respectively, of the total organic mass measured in the gas  
445 and particle phase. The molecular distribution characterized by the carbon and oxygen of these  
446 species is given in Fig. 3 (c-d). The most abundant species are characterized by a generic  
447 formula of  $C_xH_yO$  and  $C_xH_yO_2$ , resolving  $\sim 64\%$  and  $\sim 46\%$  in total of all identified species in  
448 the gas and particle phase, respectively. Another dominant component in the gas phase is  
449 hydrocarbon-like compounds ( $C_xH_y$ ) ( $\sim 27\%$ ), which contribute  $\sim 12\%$  of the organic mass in  
450 the particle phase. Species with higher oxygen numbers ( $> 2$ ) contribute to a large fraction ( $\sim$   
451  $42\%$ ) of the total particulate mass. These  $C_xH_yO_{1-4}$  groups exhibit different diurnal cycles, as  
452 shown in Fig. 4, reflecting their unique formation chemistry. The  $C_xH_y$  group peaks in the early  
453 morning rush hour and likely originates from primary traffic emissions. On the contrary, both  
454  $C_xH_yO_3$  and  $C_xH_yO_4$  groups peak at noon, suggesting a strong secondary formation source. The  
455 diurnal trends for  $C_xH_yO$  and  $C_xH_yO_2$  groups are relatively flat during the day, likely indicative  
456 of an intertwined primary emission and secondary formation processes.

457



458

459 Figure 4. Diurnal variations of observed gas-phase species with a generic formula of  $C_{2-13}H_{2-22}O_{0-4}$ . Hourly average values ( $ng\ m^{-3}$ ), together with 10<sup>th</sup>, 25<sup>th</sup>, 75<sup>th</sup>, and 90<sup>th</sup> percentiles, are  
 460 461 also plotted.

462

### 463 3.3. Measured vs. modeled gas-particle partitioning

464 Fig. 5 shows the calculated particle-phase fraction ( $F_p$ ) of the identified 152 species using  
 465 the CHARON-PTR-ToF-MS measurements in both phases. It is important to note that an  
 466 authentic standard is not required for the calculation of  $F_p$  for any given species, because the  
 467 PTR sensitivity term is essentially canceled in the divisor function in Equations (6-8). Also  
 468 given in Fig. 5 is the simulated  $F_p$  of the derived molecular formulas of all species identified  
 469 using the equilibrium partitioning theory, see method described in Section 2.4. Interestingly,  
 470 for oxidized species such as  $C_xH_yO_4$ , their measured  $F_p$  agree reasonably with the simulations,  
 471 as shown in Fig. 5a. The  $C_xH_yO_4$  group resides in the relatively higher mass range, and species

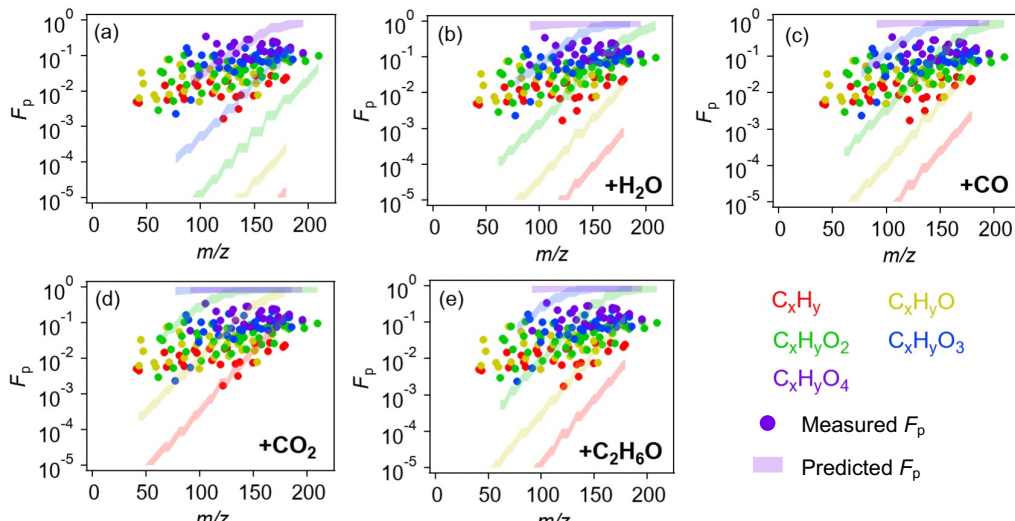
472 identified in this group are more likely actual compounds rather than fragments from larger  
473 parent molecules. Even these species dissociate into lower mass ions during PTR ionization,  
474 their calculated particle-phase fractions are unaffected by such fragmentation processes because  
475 signals of parent ions decrease by the same extent upon fragmentation in both gas and particle  
476 phases. As the oxygen number decreases, the measured  $F_p$  values tend to deviate from the  
477 simulations by up to several orders of magnitude. Note that these less oxidized compounds (e.g.,  
478  $C_xH_y$ ) are mostly small molecules and they are highly unlikely present in the condensed phase  
479 as closed-shell monomers (Pankow and Asher, 2008; Holzinger et al., 2010). Instead, they are  
480 more likely fragments produced from the decomposition of larger molecules, which no  
481 surprisingly favor partitioning in the particle phase. The discrepancy in the measurement-model  
482 comparison underscores the importance of understanding the fragmentation mechanism during  
483 PTR ionization when extracting molecular features from the raw mass spectra.

484 Parent ion fragmentation has been widely observed in PTR-MS instruments (Pagonis et al.,  
485 2019). Oxygenates exhibit trends in neutral losses of water or saturated alcohols. Here, we  
486 apply a correction to the molecular formula of the 152 identified species by assuming that these  
487 species are fragments produced from their parent precursors through the neutral losses of a  
488 carboxyl group (-CO<sub>2</sub>), a carbonyl group (-CO), a hydroxyl group (-H<sub>2</sub>O), or an alcohol group  
489 (-C<sub>2</sub>H<sub>6</sub>O). By applying this correction, the modeled  $F_p$  of a given species  $C_xH_yO_z$  would actually  
490 represent the particle-phase fraction of its parent species  $C_xH_yO_z \bullet CO_2$ ,  $C_xH_yO_z \bullet CO$ ,  
491  $C_xH_yO_z \bullet H_2O$ , or  $C_xH_yO_z \bullet C_2H_6O$ . As shown in Fig. 5 (b-e), such a correction could significantly  
492 increase the modeled  $F_p$  values by several orders of magnitude. The assumption of neutral  
493 losses of CO<sub>2</sub> or C<sub>2</sub>H<sub>6</sub>O allows for much improved agreement between modeled vs. measured  
494  $F_p$  values for less oxidized species. This implies that these small and less oxidized species are

likely fragments resulting from the decomposition of larger parent precursors. As our particle enrichment test (details given in Section 3.1) has confirmed that the thermal desorption temperature employed for particle evaporation does not lead to any intensive fragmentation, therefore the collision-induced dissociation during the proton transfer reaction process becomes the predominant process that produces fragments (Lindinger et al., 1998; Gueneron et al., 2015; Gkatzelis et al., 2018b). Although the electric field applied to the drift tube is considered low to moderate compared with most previous PTR-MS measurements ( $E/N \sim 100$  Td in this study vs.  $E/N \sim 120 - 140$  Td commonly found in PTR-MS measurements) (Pagonis et al., 2019), parent ion fragmentation was still widely observed here and complicated the mass spectra interpretation and molecular feature extraction. While some recent CHARON measurements employed lower electric field in the drift tube ( $E/N \sim 60$  Td) (Leglise et al., 2019; Gkatzelis et al., 2018a; Piel et al., 2019), such conditions could promote the formation of water cluster ions, which increase with humidity and reduce the PTR sensitivity, and therefore are not ideally suitable for our field measurements. A compromise solution would be using a moderate electric field in the drift tube (e.g.,  $\sim 100$  Td) and meanwhile applying appropriate molecular corrections to all ions detected in the mass spectra by considering possible neutral losses of small moieties. Since in this study only the information of molecular formula is derived from the PTR-MS spectra, we thus provide the lower and upper bound of the gas-particle partitioning corrections owing to neutral losses of  $\text{H}_2\text{O}$  and  $\text{CO}_2$ , respectively. In general, lower masses with higher volatilities are subject to notable changes in the particle-phase fraction as a result of neutral losses during the PTR ionization process, see detailed discussions in Text S1.

516

517



518

519 Figure 5. (a) Campaign average fraction of organic species in the particle phase ( $F_p$ ) grouped  
 520 by the oxygen number. Solid markers represent the calculated  $F_p$  based on the CHARON-PTR-  
 521 ToF-MS measurements. Colored shades represent the predicted  $F_p$  of corresponding molecular  
 522 formulas. (b-e) Measured vs. predicted  $F_p$  assuming the identified species are fragments of  
 523 corresponding parent compounds through neutral losses of  $H_2O$ ,  $CO$ ,  $CO_2$ , and  $C_2H_6O$ ,  
 524 respectively (values are given in Table S5).

525

#### 526 4. Conclusions

527 Recent studies have suggested that some of the model-measurement discrepancies in the  
 528 representation of ambient organic aerosol budget might be due to the nonequilibrium  
 529 gas/particle partitioning caused by kinetic limitations in the presence of glassy or semi-solid  
 530 phase (Perraud et al., 2012; Mai et al., 2015; Shiraiwa et al., 2013). It is therefore necessary to  
 531 validate whether the equilibrium partitioning theory could adequately describe the  
 532 condensation of semivolatile organic vapors onto atmospheric aerosols under ambient

533 conditions, and the accurate measurement of these SVOCs in both gas and particle phases is  
534 the crucial prerequisite. In this study, we have employed the PTR-ToF-MS instrument coupled  
535 to a CHARON inlet, together with a suite of complementary measurements, to characterize the  
536 atmospheric partitioning behaviors of an array of SVOCs in an urban environment of East  
537 China. Prior to the application to the field measurements, we first performed a series of  
538 laboratory experiments to test whether the CHARON inlet is capable of sampling organic  
539 molecules (including alcohols, carbonyls, and carboxylic acids) in their native states. With the  
540 low pressure condition used in the CHARON inlet, a thermal desorption temperature less than  
541 140 °C could adequately evaporate organic compounds with vapor pressure higher than  $10^{-14}$   
542 Pa while minimizing the thermal decomposition of labile functionalities. The auto-switch  
543 function between the gas and particle mode with one single PTR-ToF-MS instrument could  
544 monitor gaseous and particulate organic compounds in real time, thereby providing important  
545 information of their partitioning behaviors in the ambient atmosphere. Particle-phase fractions  
546 of a total of 152 organic species were derived from the CHARON-PTR-ToF-MS measurements  
547 and further compared with model predictions using the instantaneous equilibrium partitioning  
548 theory. While the model captured the particle-phase fraction of oxidized compounds (e.g.,  
549  $C_xH_yO_{3.4}$ ), predictions of less oxidized compounds, notably the  $C_xH_y$  family, differ from the  
550 corresponding measurements by several orders of magnitude. Such a large discrepancy is very  
551 likely caused by the intensive fragmentation of the parent organic compounds during the PTR  
552 ionization process. Accounting for common fragmentation patterns in the simulations of gas-  
553 particle partitioning, for example, neutral losses of  $-CO_2$ ,  $-CO$ ,  $-H_2O$ , or  $-C_2H_6O$ , could largely  
554 improve the model-measurement agreement. Such corrections are very necessary towards an  
555 accurate measurement of both particle- and gas-phase SVOCs using the CHARON-PTR-ToF-

556 MS instrument. Our study suggests the crucial importance of optimizing operation conditions  
557 and understanding the fragmentation mechanism in the particle collection, vaporization, and  
558 ionization processes in understanding the gas-particle partitioning of organic compounds using  
559 any thermal desorption based aerosol measurement method.

560

561 *Data availability.* The data shown in the paper are available upon request from the  
562 corresponding author.

563 *Author Contributions.* YP carried out experiments and measurements and drafted the  
564 manuscript. HW and XZ designed the experimental studies, supervised the laboratory work and  
565 wrote the manuscript. YG and SJ supported the ambient measurements. SZ, DH, PH, and SL  
566 supported the data analysis. TC and CH supervised the scientific work. All authors have given  
567 approval to the final version of the manuscript.

568 *Competing interests.* The authors declare no competing financial interest.

569 *Acknowledgements.* This research has been supported by the National Natural Science  
570 Foundation of China (No. 42175135, No. 42175179) and the Shanghai Science and Technology  
571 Commission of the Shanghai Municipality (No. 20ZR1447800).

572

### 573 **References**

574 Antonsen, S., Bunkan, A. J. C., D'Anna, B., Eichler, P., Farren, N., Hallquist, M., Hamilton, J.  
575 F., Kvarnliden, H., Mikoviny, T., Muller, M., Nielsen, C. J., Stenstrom, Y., Tan, W., Wisthaler,  
576 A., and Zhu, L.: Atmospheric chemistry of tert-butylamine and AMP, in: Enrgy Proced, edited  
577 by: Dixon, T., Laloui, L., and Twinning, S., Energy Procedia, Elsevier Science Bv, Amsterdam,  
578 1026-1032, 10.1016/j.egypro.2017.03.1248, 2017.

579 Crounse, J. D., McKinney, K. A., Kwan, A. J., and Wennberg, P. O.: Measurement of gas-phase

580 hydroperoxides by chemical ionization mass spectrometry, *Anal. Chem.*, 78, 6726-6732,  
581 10.1021/ac0604235, 2006.

582 de Gouw, J. and Warneke, C.: Measurements of volatile organic compounds in the earths  
583 atmosphere using proton-transfer-reaction mass spectrometry, *Mass Spectrometry Reviews*, 26,  
584 223-257, 10.1002/mas.20119, 2007.

585 Donahue, N. M., Epstein, S. A., Pandis, S. N., and Robinson, A. L.: A two-dimensional  
586 volatility basis set: 1. organic-aerosol mixing thermodynamics, *Atmos. Chem. Phys.*, 11, 3303-  
587 3318, 10.5194/acp-11-3303-2011, 2011.

588 Eichler, P., Muller, M., D'Anna, B., and Wisthaler, A.: A novel inlet system for online chemical  
589 analysis of semi-volatile submicron particulate matter, *Atmos. Meas. Tech.*, 8, 1353-1360,  
590 10.5194/amt-8-1353-2015, 2015.

591 Eichler, P., Muller, M., Rohmann, C., Stengel, B., Orasche, J., Zimmermann, R., and Wisthaler,  
592 A.: Lubricating Oil as a Major Constituent of Ship Exhaust Particles, *Environ. Sci. Technol.*  
593 Lett., 4, 54-58, 10.1021/acs.estlett.6b00488, 2017.

594 EPA: Estimation Program Interface (EPI) Suite (v4.11), US [code], 2012.

595 Francis, G. J., Milligan, D. B., and McEwan, M. J.: Gas-Phase Reactions and Rearrangements  
596 of Alkyl Esters with H<sub>3</sub>O<sup>+</sup>, NO<sup>+</sup>, and O<sub>2</sub>•<sup>+</sup>: A Selected Ion Flow Tube Study, *J. Phys. Chem.*  
597 A, 111, 9670-9679, 10.1021/jp0731304, 2007.

598 Gkatzelis, G. I., Tillmann, R., Hohaus, T., Muller, M., Eichler, P., Xu, K. M., Schlag, P., Schmitt,  
599 S. H., Wegener, R., Kaminski, M., Holzinger, R., Wisthaler, A., and Kiendler-Scharr, A.:  
600 Comparison of three aerosol chemical characterization techniques utilizing PTR-ToF-MS: a  
601 study on freshly formed and aged biogenic SOA, *Atmos. Meas. Tech.*, 11, 1481-1500, 2018a.

602 Gkatzelis, G. I., Hohaus, T., Tillmann, R., Gensch, I., Muller, M., Eichler, P., Xu, K. M., Schlag,  
603 P., Schmitt, S. H., Yu, Z. J., Wegener, R., Kaminski, M., Holzinger, R., Wisthaler, A., and  
604 Kiendler-Scharr, A.: Gas-to-particle partitioning of major biogenic oxidation products: a study  
605 on freshly formed and aged biogenic SOA, *Atmos. Chem. Phys.*, 18, 12969-12989,  
606 10.5194/acp-18-12969-2018, 2018b.

607 Gueneron, M., Erickson, M. H., VanderSchelden, G. S., and Jobson, B. T.: PTR-MS  
608 fragmentation patterns of gasoline hydrocarbons, *International Journal of Mass Spectrometry*,

609 379, 97-109, 10.1016/j.ijms.2015.01.001, 2015.

610 He, X., Wang, Q., Huang, X. H. H., Huang, D. D., Zhou, M., Qiao, L., Zhu, S., Ma, Y.-g., Wang,  
611 H.-l., Li, L., Huang, C., Xu, W., Worsnop, D. R., Goldstein, A. H., and Yu, J. Z.: Hourly  
612 measurements of organic molecular markers in urban Shanghai, China: Observation of  
613 enhanced formation of secondary organic aerosol during particulate matter episodic periods,  
614 *Atmos. Environ.*, 240, 10.1016/j.atmosenv.2020.117807, 2020.

615 Heald, C. L. and Kroll, J. H.: The fuel of atmospheric chemistry: Toward a complete description  
616 of reactive organic carbon, *Sci. Adv.*, 6, 10.1126/sciadv.aay8967, 2020.

617 Holzinger, R., Goldstein, A. H., Hayes, P. L., Jimenez, J. L., and Timkovsky, J.: Chemical  
618 evolution of organic aerosol in Los Angeles during the CalNex 2010 study, *Atmos. Chem. Phys.*,  
619 13, 10125-10141, 10.5194/acp-13-10125-2013, 2013.

620 Holzinger, R., Williams, J., Herrmann, F., Lelieveld, J., Donahue, N. M., and Rockmann, T.:  
621 Aerosol analysis using a Thermal-Desorption Proton-Transfer-Reaction Mass Spectrometer  
622 (TD-PTR-MS): a new approach to study processing of organic aerosols, *Atmos. Chem. Phys.*,  
623 10, 2257-2267, 10.5194/acp-10-2257-2010, 2010.

624 Holzinger, R., Acton, W. J. F., Bloss, W. J., Breitenlechner, M., Crilley, L. R., Dusanter, S.,  
625 Gonin, M., Gros, V., Keutsch, F. N., Kiendler-Scharr, A., Kramer, L. J., Krechmer, J. E.,  
626 Languille, B., Locoge, N., Lopez-Hilfiker, F., Materić, D., Moreno, S., Nemitz, E., Quéléver,  
627 L. L. J., Sarda Esteve, R., Sauvage, S., Schallhart, S., Sommariva, R., Tillmann, R., Wedel, S.,  
628 Worton, D. R., Xu, K., and Zaytsev, A.: Validity and limitations of simple reaction kinetics to  
629 calculate concentrations of organic compounds from ion counts in PTR-MS, *Atmos. Meas. Tech.*,  
630 12, 6193-6208, 10.5194/amt-12-6193-2019, 2019.

631 Huang, D. D., Zhu, S., An, J., Wang, Q., Qiao, L., Zhou, M., He, X., Ma, Y., Sun, Y., Huang,  
632 C., Yu, J. Z., and Zhang, Q.: Comparative Assessment of Cooking Emission Contributions to  
633 Urban Organic Aerosol Using Online Molecular Tracers and Aerosol Mass Spectrometry  
634 Measurements, *Environ. Sci. Technol.*, 10.1021/acs.est.1c03280, 2021.

635 Huang, G., Liu, Y., Shao, M., Li, Y., Chen, Q., Zheng, Y., Wu, Z., Liu, Y., Wu, Y., Hu, M., Li,  
636 X., Lu, S., Wang, C., Liu, J., Zheng, M., and Zhu, T.: Potentially Important Contribution of  
637 Gas-Phase Oxidation of Naphthalene and Methylnaphthalene to Secondary Organic Aerosol  
638 during Haze Events in Beijing, *Environ. Sci. Technol.*, 53, 1235-1244, 10.1021/acs.est.8b04523,

639 2019.

640 Inomata, S., Sato, K., Hirokawa, J., Sakamoto, Y., Tanimoto, H., Okumura, M., Tohno, S., and  
641 Imamura, T.: Analysis of secondary organic aerosols from ozonolysis of isoprene by proton  
642 transfer reaction mass spectrometry, *Atmos. Environ.*, 97, 397-405,  
643 10.1016/j.atmosenv.2014.03.045, 2014.

644 Krechmer, J. E., Groessl, M., Zhang, X., Junninen, H., Massoli, P., Lambe, A. T., Kimmel, J.  
645 R., Cubison, M. J., Graf, S., Lin, Y.-H., Budisulistiorini, S. H., Zhang, H., Surratt, J. D.,  
646 Knochenmuss, R., Jayne, J. T., Worsnop, D. R., Jimenez, J.-L., and Canagaratna, M. R.: Ion  
647 mobility spectrometry–mass spectrometry (IMS–MS) for on- and offline analysis of  
648 atmospheric gas and aerosol species, *Atmos. Meas. Tech.*, 9, 3245-3262, 10.5194/amt-9-3245-  
649 2016, 2016.

650 Le Breton, M., Wang, Y. J., Hallquist, A. M., Pathak, R. K., Zheng, J., Yang, Y. D., Shang, D.  
651 J., Glasius, M., Bannan, T. J., Liu, Q. Y., Chan, C. K., Percival, C. J., Zhu, W. F., Lou, S. R.,  
652 Topping, D., Wang, Y. C., Yu, J. Z., Lu, K. D., Guo, S., Hu, M., and Hallquist, M.: Online gas-  
653 and particle-phase measurements of organosulfates, organosulfonates and nitrooxy  
654 organosulfates in Beijing utilizing a FIGAERO ToF-CIMS, *Atmos. Chem. Phys.*, 18, 10355-  
655 10371, 2018.

656 Lee, B. H., Lopez-Hilfiker, F. D., D'Ambro, E. L., Zhou, P., Boy, M., Petäjä, T., Hao, L.,  
657 Virtanen, A., and Thornton, J. A.: Semi-volatile and highly oxygenated gaseous and particulate  
658 organic compounds observed above a boreal forest canopy, *Atmos. Chem. Phys.*, 18, 11547-  
659 11562, 10.5194/acp-18-11547-2018, 2018.

660 Leglise, J., Muller, M., Piel, F., Otto, T., and Wisthaler, A.: Bulk Organic Aerosol Analysis by  
661 Proton-Transfer-Reaction Mass Spectrometry: An Improved Methodology for the  
662 Determination of Total Organic Mass, O:C and H:C Elemental Ratios, and the Average  
663 Molecular Formula, *Anal. Chem.*, 91, 12619-12624, 10.1021/acs.analchem.9b02949, 2019.

664 Lindinger, W., Hansel, A., and Jordan, A.: Proton-transfer-reaction mass spectrometry (PTR-  
665 MS): on-line monitoring of volatile organic compounds at pptv levels, *Chem. Soc. Rev.*, 27,  
666 347-354, 10.1039/a827347z, 1998.

667 Lopez-Hilfiker, F. D., Mohr, C., Ehn, M., Rubach, F., Kleist, E., Wildt, J., Mentel, T. F., Lutz,  
668 A., Hallquist, M., Worsnop, D., and Thornton, J. A.: A novel method for online analysis of gas

669 and particle composition: description and evaluation of a Filter Inlet for Gases and AEROSols  
670 (FIGAERO), *Atmos. Meas. Tech.*, 7, 983-1001, 10.5194/amt-7-983-2014, 2014.

671 Lopez-Hilfiker, F. D., Mohr, C., Ehn, M., Rubach, F., Kleist, E., Wildt, J., Mentel, T. F.,  
672 Carrasquillo, A. J., Daumit, K. E., Hunter, J. F., Kroll, J. H., Worsnop, D. R., and Thornton, J.  
673 A.: Phase partitioning and volatility of secondary organic aerosol components formed from  $\alpha$ -  
674 pinene ozonolysis and OH oxidation: the importance of accretion products and other low  
675 volatility compounds, *Atmos. Chem. Phys.*, 15, 7765-7776, 10.5194/acp-15-7765-2015, 2015.

676 Lopez-Hilfiker, F. D., Mohr, C., D'Ambro, E. L., Lutz, A., Riedel, T. P., Gaston, C. J., Iyer, S.,  
677 Zhang, Z., Gold, A., Surratt, J. D., Lee, B. H., Kurten, T., Hu, W. W., Jimenez, J., Hallquist, M.,  
678 and Thornton, J. A.: Molecular Composition and Volatility of Organic Aerosol in the  
679 Southeastern U.S.: Implications for IEPOX Derived SOA, *Environ. Sci. Technol.*, 50, 2200-  
680 2209, 10.1021/acs.est.5b04769, 2016.

681 Lutz, A., Mohr, C., Le Breton, M., Lopez-Hilfiker, F. D., Priestley, M., Thornton, J. A., and  
682 Hallquist, M.: Gas to Particle Partitioning of Organic Acids in the Boreal Atmosphere, *ACS*  
683 *Earth Space Chem.*, 3, 1279-1287, 10.1021/acsearthspacechem.9b00041, 2019.

684 Mai, H., Shiraiwa, M., Flagan, R. C., and Seinfeld, J. H.: Under What Conditions Can  
685 Equilibrium Gas-Particle Partitioning Be Expected to Hold in the Atmosphere?, *Environ. Sci.*  
686 *Technol.*, 49, 11485-11491, 10.1021/acs.est.5b02587, 2015.

687 Muller, M., Eichler, P., D'Anna, B., Tan, W., and Wisthaler, A.: Direct Sampling and Analysis  
688 of Atmospheric Particulate Organic Matter by Proton-Transfer-Reaction Mass Spectrometry,  
689 *Anal. Chem.*, 89, 10889-10897, 10.1021/acs.analchem.7b02582, 2017.

690 Pagonis, D., Sekimoto, K., and de Gouw, J.: A Library of Proton-Transfer Reactions of  $\text{H}_3\text{O}^+$   
691 Ions Used for Trace Gas Detection, *Journal of the American Society for Mass Spectrometry*, 30,  
692 1330-1335, 10.1007/s13361-019-02209-3, 2019.

693 Palm, B. B., Peng, Q. Y., Fredrickson, C. D., Lee, B., Garofalo, L. A., Pothier, M. A.,  
694 Kreidenweis, S. M., Farmer, D. K., Pokhrel, R. P., Shen, Y. J., Murphy, S. M., Permar, W., Hu,  
695 L., Campos, T. L., Hall, S. R., Ullmann, K., Zhang, X., Flocke, F., Fischer, E. V., and Thornton,  
696 J. A.: Quantification of organic aerosol and brown carbon evolution in fresh wildfire plumes,  
697 *Proc Natl Acad Sci U S A*, 117, 29469-29477, 10.1073/pnas.2012218117, 2020.

698 Pankow, J. F.: An absorption-model of the gas aerosol partitioning involved in the formation of

699 secondary organic aerosol, *Atmos. Environ.*, 28, 189-193, 10.1016/1352-2310(94)90094-9,  
700 1994.

701 Pankow, J. F. and Asher, W. E.: SIMPOL.1: a simple group contribution method for predicting  
702 vapor pressures and enthalpies of vaporization of multifunctional organic compounds, *Atmos.*  
703 *Chem. Phys.*, 8, 2773-2796, 10.5194/acp-8-2773-2008, 2008.

704 Peng, Y., Wang, H., Wang, Q., Jing, S., An, J., Gao, Y., Huang, C., Yan, R., Dai, H., Cheng, T.,  
705 Zhang, Q., Li, M., Hu, J., Shi, Z., Li, L., Lou, S., Tao, S., Hu, Q., Lu, J., and Chen, C.:  
706 Observation-based sources evolution of non-methane hydrocarbons (NMHCs) in a megacity of  
707 China, *J. Environ. Sci.*, 124, 794-805, 10.1016/j.jes.2022.01.040, 2023.

708 Perraud, V., Bruns, E. A., Ezell, M. J., Johnson, S. N., Yu, Y., Alexander, M. L., Zelenyuk, A.,  
709 Imre, D., Chang, W. L., Dabdub, D., Pankow, J. F., and Finlayson-Pitts, B. J.: Nonequilibrium  
710 atmospheric secondary organic aerosol formation and growth, *Proc Natl Acad Sci U S A*, 109,  
711 2836-2841, 10.1073/pnas.1119909109, 2012.

712 Piel, F., Muller, M., Mikoviny, T., Pusede, S. E., and Wisthaler, A.: Airborne measurements of  
713 particulate organic matter by proton-transfer-reaction mass spectrometry (PTR-MS): a pilot  
714 study, *Atmos. Meas. Tech.*, 12, 5947-5958, 10.5194/amt-12-5947-2019, 2019.

715 Piel, F., Müller, M., Winkler, K., Skytte af Sätra, J., and Wisthaler, A.: Introducing the extended  
716 volatility range proton-transfer-reaction mass spectrometer (EVR PTR-MS), *Atmos. Meas.*  
717 *Tech.*, 14, 1355-1363, 10.5194/amt-14-1355-2021, 2021.

718 Sekimoto, K., Li, S. M., Yuan, B., Koss, A., Coggon, M., Warneke, C., and de Gouw, J.:  
719 Calculation of the sensitivity of proton-transfer-reaction mass spectrometry (PTR-MS) for  
720 organic trace gases using molecular properties, *International Journal of Mass Spectrometry*, 421,  
721 71-94, 10.1016/j.ijms.2017.04.006, 2017.

722 Shiraiwa, M. and Seinfeld, J. H.: Equilibration timescale of atmospheric secondary organic  
723 aerosol partitioning, *Geophysical Research Letters*, 39, n/a-n/a, 10.1029/2012gl054008, 2012.

724 Shiraiwa, M., Zuend, A., Bertram, A. K., and Seinfeld, J. H.: Gas-particle partitioning of  
725 atmospheric aerosols: interplay of physical state, non-ideal mixing and morphology, *Phys.*  
726 *Chem. Chem. Phys.*, 15, 11441-11453, 10.1039/c3cp51595h, 2013.

727 Spanel, P. and Smith, D.: SIFT studies of the reactions of H<sub>3</sub>O<sup>+</sup>, NO<sup>+</sup> and O<sub>2</sub><sup>+</sup> with a series

728 of alcohols, Int. J. Mass Spectrom. Ion Processes, 167-168, 375-388,  
729 [https://doi.org/10.1016/S0168-1176\(97\)00085-2](https://doi.org/10.1016/S0168-1176(97)00085-2), 1997.

730 Spanel, P., Ji, Y. F., and Smith, D.: SIFT studies of the reactions of H<sub>3</sub>O<sup>+</sup>, NO<sup>+</sup> and O<sub>2</sub>(<sup>+</sup>)  
731 with a series of aldehydes and ketones, International Journal of Mass Spectrometry, 165, 25-  
732 37, 10.1016/s0168-1176(97)00166-3, 1997.

733 Stark, H., Yatavelli, R. L. N., Thompson, S. L., Kang, H., Krechmer, J. E., Kimmel, J. R., Palm,  
734 B. B., Hu, W. W., Hayes, P. L., Day, D. A., Campuzano-Jost, P., Canagaratna, M. R., Jayne, J.  
735 T., Worsnop, D. R., and Jimenez, J. L.: Impact of Thermal Decomposition on Thermal  
736 Desorption Instruments: Advantage of Thermogram Analysis for Quantifying Volatility  
737 Distributions of Organic Species, Environ. Sci. Technol., 51, 8491-8500,  
738 10.1021/acs.est.7b00160, 2017.

739 Tan, W., Zhu, L., Mikoviny, T., Nielsen, C. J., Wisthaler, A., Eichler, P., Muller, M., D'Anna,  
740 B., Farren, N. J., Hamilton, J. F., Pettersson, J. B. C., Hallquist, M., Antonsen, S., and Stenstrom,  
741 Y.: Theoretical and Experimental Study on the Reaction of tert-Butylamine with OH Radicals  
742 in the Atmosphere, J. Phys. Chem. A, 122, 4470-4480, 10.1021/acs.jpca.8b01862, 2018.

743 Tani, A., Hayward, S., and Hewitta, C. N.: Measurement of monoterpenes and related  
744 compounds by proton transfer reaction-mass spectrometry (PTR-MS), International Journal of  
745 Mass Spectrometry, 223, 561-578, 10.1016/s1387-3806(02)00880-1, 2003.

746 Thompson, S. L., Yatavelli, R. L. N., Stark, H., Kimmel, J. R., Krechmer, J. E., Day, D. A., Hu,  
747 W., Isaacman-VanWertz, G., Yee, L., Goldstein, A. H., Khan, M. A. H., Holzinger, R., Kreisberg,  
748 N., Lopez-Hilfiker, F. D., Mohr, C., Thornton, J. A., Jayne, J. T., Canagaratna, M., Worsnop, D.  
749 R., and Jimenez, J. L.: Field intercomparison of the gas/particle partitioning of oxygenated  
750 organics during the Southern Oxidant and Aerosol Study (SOAS) in 2013, Aerosol Sci. Technol.,  
751 51, 30-56, 10.1080/02786826.2016.1254719, 2016.

752 Veres, P., Roberts, J. M., Warneke, C., Welsh-Bon, D., Zahniser, M., Herndon, S., Fall, R., and  
753 de Gouw, J.: Development of negative-ion proton-transfer chemical-ionization mass  
754 spectrometry (NI-PT-CIMS) for the measurement of gas-phase organic acids in the atmosphere,  
755 International Journal of Mass Spectrometry, 274, 48-55, 10.1016/j.ijms.2008.04.032, 2008.

756 Voliotis, A., Wang, Y., Shao, Y., Du, M., Bannan, T. J., Percival, C. J., Pandis, S. N., Alfarra, M.  
757 R., and McFiggans, G.: Exploring the composition and volatility of secondary organic aerosols

758 in mixed anthropogenic and biogenic precursor systems, *Atmos. Chem. Phys.*, 21, 14251-14273,  
759 10.5194/acp-21-14251-2021, 2021.

760 Wang, H. L., Lou, S. R., Huang, C., Qiao, L. P., Tang, X. B., Chen, C. H., Zeng, L. M., Wang,  
761 Q., Zhou, M., Lu, S. H., and Yu, X. N.: Source Profiles of Volatile Organic Compounds from  
762 Biomass Burning in Yangtze River Delta, China, *Aerosol Air Qual. Res.*, 14, 818-828,  
763 10.4209/aaqr.2013.05.0174, 2014.

764 Wang, M. Y., Chen, D. X., Xiao, M., Ye, Q., Stolzenburg, D., Hofbauer, V., Ye, P. L., Vogel, A.  
765 L., Mauldin, R. L., Amorim, A., Baccarini, A., Baumgartner, B., Brilke, S., Dada, L., Dias, A.,  
766 Duplissy, J., Finkenzeller, H., Garmash, O., He, X. C., Hoyle, C. R., Kim, C., Kvashnin, A.,  
767 Lehtipalo, K., Fischer, L., Molteni, U., Petaja, T., Pospisilova, V., Quelever, L. L. J., Rissanen,  
768 M., Simon, M., Tauber, C., Tome, A., Wagner, A. C., Weitz, L., Volkamer, R., Winkler, P. M.,  
769 Kirkby, J., Worsnop, D. R., Kulmala, M., Baltensperger, U., Dommen, J., El Haddad, I., and  
770 Donahue, N. M.: Photo-oxidation of Aromatic Hydrocarbons Produces Low-Volatility Organic  
771 Compounds, *Environ. Sci. Technol.*, 54, 7911-7921, 2020a.

772 Wang, Q. Q., He, X., Zhou, M., Huang, D. D., Qiao, L. P., Zhu, S. H., Ma, Y. G., Wang, H. L.,  
773 Li, L., Huang, C., Huang, X. H. H., Xu, W., Worsnop, D., Goldstein, A. H., Guo, H., and Yu, J.  
774 Z.: Hourly Measurements of Organic Molecular Markers in Urban Shanghai, China: Primary  
775 Organic Aerosol Source Identification and Observation of Cooking Aerosol Aging, *ACS Earth  
776 Space Chem.*, 4, 1670-1685, 2020b.

777 Yatavelli, R. L. N., Lopez-Hilfiker, F., Wargo, J. D., Kimmel, J. R., Cubison, M. J., Bertram, T.  
778 H., Jimenez, J. L., Gonin, M., Worsnop, D. R., and Thornton, J. A.: A Chemical Ionization  
779 High-Resolution Time-of-Flight Mass Spectrometer Coupled to a Micro Orifice Volatilization  
780 Impactor (MOVI-HRToF-CIMS) for Analysis of Gas and Particle-Phase Organic Species,  
781 *Aerosol Sci. Technol.*, 46, 1313-1327, 2012.

782 Ye, C., Yuan, B., Lin, Y., Wang, Z., Hu, W., Li, T., Chen, W., Wu, C., Wang, C., Huang, S., Qi,  
783 J., Wang, B., Wang, C., Song, W., Wang, X., Zheng, E., Krechmer, J. E., Ye, P., Zhang, Z., Wang,  
784 X., Worsnop, D. R., and Shao, M.: Chemical characterization of oxygenated organic  
785 compounds in the gas phase and particle phase using iodide CIMS with FIGAERO in urban air,  
786 *Atmos. Chem. Phys.*, 21, 8455-8478, 10.5194/acp-21-8455-2021, 2021.

787 Zhang, X. and Seinfeld, J. H.: A functional group oxidation model (FGOM) for SOA formation  
788 and aging, *Atmos. Chem. Phys.*, 13, 5907-5926, 10.5194/acp-13-5907-2013, 2013.

789 Zhang, X., Dalleska, N. F., Huang, D. D., Bates, K. H., Sorooshian, A., Flagan, R. C., and  
790 Seinfeld, J. H.: Time-resolved molecular characterization of organic aerosols by PILS plus  
791 UPLC/ESI-Q-TOFMS, *Atmos. Environ.*, 130, 180-189, 10.1016/j.atmosenv.2015.08.049,  
792 2016a.

793 Zhang, X., Zhang, H. F., Xu, W., Wu, X. K., Tyndall, G. S., Orlando, J. J., Jayne, J. T., Worsnop,  
794 D. R., and Canagaratna, M. R.: Molecular characterization of alkyl nitrates in atmospheric  
795 aerosols by ion mobility mass spectrometry, *Atmos. Meas. Tech.*, 12, 5535-5545, 10.5194/amt-  
796 12-5535-2019, 2019.

797 Zhang, X., Krechmer, J. E., Groessl, M., Xu, W., Graf, S., Cubison, M., Jayne, J. T., Jimenez,  
798 J. L., Worsnop, D. R., and Canagaratna, M. R.: A novel framework for molecular  
799 characterization of atmospherically relevant organic compounds based on collision cross  
800 section and mass-to-charge ratio, *Atmos. Chem. Phys.*, 16, 12945-12959, 10.5194/acp-16-  
801 12945-2016, 2016b.

802 Zhao, Y. L., Kreisberg, N. M., Worton, D. R., Isaacman, G., Weber, R. J., Liu, S., Day, D. A.,  
803 Russell, L. M., Markovic, M. Z., VandenBoer, T. C., Murphy, J. G., Hering, S. V., and Goldstein,  
804 A. H.: Insights into Secondary Organic Aerosol Formation Mechanisms from Measured  
805 Gas/Particle Partitioning of Specific Organic Tracer Compounds, *Environ. Sci. Technol.*, 47,  
806 3781-3787, 2013.

807 Zhu, H., Wang, H., Jing, S., Wang, Y., Cheng, T., Tao, S., Lou, S., Qiao, L., Li, L., and Chen,  
808 J.: Characteristics and sources of atmospheric volatile organic compounds (VOCs) along the  
809 mid-lower Yangtze River in China, *Atmos. Environ.*, 190, 232-240,  
810 10.1016/j.atmosenv.2018.07.026, 2018.

811 Zhu, S., Wang, Q., Qiao, L., Zhou, M., Wang, S., Lou, S., Huang, D., Wang, Q., Jing, S., Wang,  
812 H., Chen, C., Huang, C., and Yu, J. Z.: Tracer-based characterization of source variations of  
813 PM2.5 and organic carbon in Shanghai influenced by the COVID-19 lockdown, *Faraday  
814 Discuss.*, 226, 112-137, 10.1039/d0fd00091d, 2021.

815